The bichromatic excitable Schrodinger metamedium

Ekaterina Ostheimer[1], Valery Labunets[2], and Ivan Artemov[2]

[1] Capricat LLC, Florida, USA
katya@capricat.com
[2] Ural Federal University, Yekaterinburg, Russia
vlabunets05@yahoo.com

Abstract. In this work, we apply quantum cellular automata (QCA) to study pattern formation and image processing in quantum-diffusion Schrodinger systems (QDSS) with generalized complex diffusion coefficients. Generalized complex numbers have the real part and imaginary part with the imaginary unit $i^2 = -1$ (classical case), $i^2 = +1$ (double numbers) and $i^2 = 0$ (dual numbers). They form three 2-D complex algebras. Discretization of the Schrodinger equation gives "lattice based metamaterial models" with various complex–valued physical parameters. The process of excitation in these media is described by the Schrodinger equations with the wave functions that have values in algebras of the complex, dual, double numbers. If a traditional computer is thought of as a "programmable object", QDSS in the form of QCA is a computer of new kind and is better visualized as a "programmable material". The purpose of this work is to introduce new metamedium in the form of cellular automata. The cells are placed in a 2-D array and they are capable of performing basic complex operating (in different complex algebras) and exchanging messages about their state. Cellular automata like architectures have been successfully used for computer vision problems and grey-level image processing. Such media possess large opportunities in processing of bichromatic images in comparison with the ordinary diffusion media with the real-valued diffusion coefficients. The latter media are used for creation of the eye-prosthesis (so called the "silicon eye"). The medium suggested can serve as the prosthesis prototype for perception of the bichromatic images.

Keywords: image processing, Schrodinger equation, complex diffusion, cellular automata, Minkowski geometry, Galilean geometry, metamedium

Introduction

We examine a graphical representation of 2D Schrodinger equation solution found with performing several cellular automata iterations. Initial conditions for the equation are the same every time: we use a black square image with a white point in the middle (it is the only cell in the automata that is not equal

to zero in the beginning). The only exception is the experiment with moving particle, that will be described in the last section. More basic information about cellular automata, such as it's application and properties, can be found in [1]

Cellular automata is a more fast, demonstrative and easy way of modeling a metamedium than the method of the straight equation solving. We aren't the first men who use a cellular automata for such purposes. For example, in [2] and [3] it is described how to use a quantum cellular automata for image processing. Of course, we can achieve good results in image segmentation and edge detection using QCA, but nobody proved that QCA with a "true imaginary" diffusion coefficient D will provide the best output. That's why it is important to start researching QCAs with more general properties, where D is an ordinary complex number with the phase that isn't equal to $90°$.

We use well known expression for Schrodinger equation as the basis:

$$\frac{d}{dt}\phi = D \cdot \left(\frac{d^2}{dx^2}\phi + \frac{d^2}{dy^2}\phi \right), \tag{1}$$

where $\phi(x, y, t)$ is a complex value of a cell, that is located at point with coordinates (x, y) at time (or iteration number) t; D is a complex diffusion coefficient.

For our discrete cellular implementation it useful to represent the Laplacian in the braces in a different way:

$$\frac{d^2}{dx^2}\phi = \phi(x+1, y, t) + \phi(x-1, y, t) - 2\phi(x, y, t), \tag{2}$$

$$\frac{d^2}{dy^2}\phi = \phi(x, y+1, t) + \phi(x, y-1, t) - 2\phi(x, y, t), \tag{3}$$

$$\frac{d}{dt}\phi = \phi(x, y, t+1) - \phi(x, y, t). \tag{4}$$

As a result we can obtain the expression for a cell state at the next iteration:

$$\begin{aligned} \phi(x, y, t+1) = \phi(x, y, t) + D \cdot (\phi(x+1, y, t) + \\ + \phi(x-1, y, t) + \phi(x, y+1, t) + \phi(x, y-1, t) - 4\phi(x, y, t)). \end{aligned} \tag{5}$$

It can be seen, that the last expressions implicitly contains a matrix of weight coefficients, that is frequently used in image processing for edge detection purposes in so-called Laplacian filter (see [4]):

$$\left[\begin{array}{c|c|c} 0 \cdot \phi(x-1, y+1, t) & 1 \cdot \phi(x, y+1, t) & 0 \cdot \phi(x+1, y+1, t) \\ \hline 1 \cdot \phi(x-1, y, t) & -4 \cdot \phi(x, y, t) & 1 \cdot \phi(x+1, y, t) \\ \hline 0 \cdot \phi(x-1, y-1, t) & 1 \cdot \phi(x, y-1, t) & 0 \cdot \phi(x+1, y-1, t) \end{array}\right] \rightarrow \left[\begin{array}{c|c|c} 0 & 1 & 0 \\ \hline 1 & -4 & 1 \\ \hline 0 & 1 & 0 \end{array}\right]. \tag{6}$$

In this matrix we use only four closes neighbors of the central cell in the automata. More accurate and complex matrix masks can be found for the approximation of laplacian (for example, see 'diamond mask' in [5]).

1 Influence of diffusion coefficient's phase for Euclidean geometry

We will use a fixed D's absolute value, because it only has an impact on visualization. We needed to find such $|D|$, that will provide quite fast propagation processes, but will not cause an overflow because of extremely high values. $|D| = 0.11$ is very convenient for our purposes.

For a standard complex plane geometry we use ordinary formulas, that we show only for a comparison with different "exotic" geometries. Let Z be a complex number, R - a real number, ϕ - an angle in radians, $i_{-1} = i : i^2 = -1$ then

$$Z = R \cdot (cos(\phi) + i_{-1} \cdot sin(\phi)); \qquad |Z| = \sqrt{(Re\{Z\})^2 + (Im\{Z\})^2}; \quad (7)$$

$$Re\{Z\} = R \cdot cos(\phi); \qquad Im\{Z\} = R \cdot sin(\phi). \quad (8)$$

On Fig. 1 and Fig. 2 you can see the modeling results for complex coefficient D with it's different phase values. Obviously, if $arg\{D\} = 0°$ and we assign a

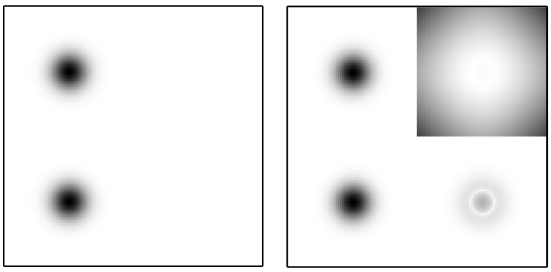

Fig. 1. 128th iteration of complex diffusion for D's phases $0°$ (left image) and $5°$ (right image) using $i^2 = -1$

value $Z_{excited} = 1 + j \cdot 0$ to the cell, that is just excited, then we will not have any nonzero values for imaginary and phase components of all cells. It corresponds to the heat equation realization (see [6]).

The final images were inverted to decrease the amount of black color for better visual perception, so big values correspond darker points.

Each image on our figures consists of four quads, that represent absolute values of complex numbers in cells (top left quad), their phases (top right one), real parts (bottom left one) and imaginary parts (bottom right quad).

It can be seen on Fig. 2 (right part), that real and imaginary parts are fluctuating in antiphase (white rings in the bottom quads aren't at the same position: they are located between each other). It causes a smooth decreasing complex module picture: there are no white rings of zero absolute value on it. If we take a 'slice' of the left top quads then we will see, that cell's absolute value is decreasing under the law of the Gaussian curve (see Fig. 3).

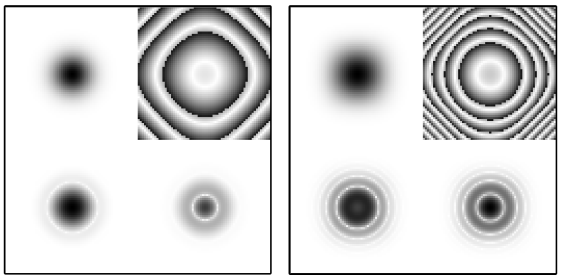

Fig. 2. 128th iteration of complex diffusion for D's phases 25° and 60° using $i^2 = -1$

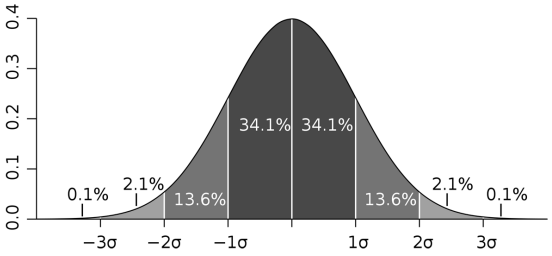

Fig. 3. A Gaussian curve showing normalized cell's absolute value distribution

2 Schrodinger equation for Minkowski geometry

For Minkowski geometry we have to use hyperbolic functions instead of ordinary trigonometric ones [7]. If $i_{+1} = i : i^2 = +1$ then

$$Z = R \cdot (cosh(\phi) + i_{+1} \cdot sinh(\phi)); \qquad |Z| = \sqrt{(Re\{Z\})^2 - (Im\{Z\})^2}; \tag{9}$$

$$Re\{Z\} = R \cdot cosh(\phi); \qquad Im\{Z\} = R \cdot sinh(\phi). \tag{10}$$

The unit circle for a complex plane with Minkowski geometry have an absolutely different shape. It has the form of a hyperbola (see Fig. 4). That's why we have to use hyperbolic functions to get a complex number's coordinate on 2-D plane. Also it is very important, that now we have a subtraction operation in the expression for Z's absolute value. It leads to the possibility of complex-valued modules. For uniform visualization purposes, we take either real or imaginary part of $|Z|$ respectively.

On Fig. 5 you can see the modeling results for the same initial conditions (a single excited central cell) in Minkowski geometry for small phase values.

Note, that there are no more waves in real and phase parts of our cellular array. The amount of waves in the imaginary parts section isn't increasing with growth of D's phase. The ring of high phase values appears in the top right quad.

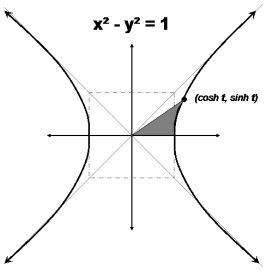

Fig. 4. Hyperbola is the unit "circle" for the Minkowski geometry

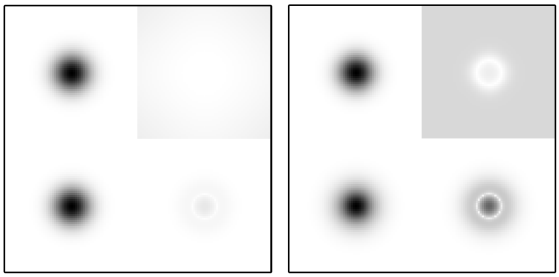

Fig. 5. 128th iteration of complex diffusion for D's phases 5° and 20° using $i^2 = +1$

3 Complex diffusion coefficient for Galilean geometry

Galilean geometry provides us with the simplest formulas for complex numbers at new complex plane [8]. If $i_0 = i : i^2 = 0$ then

$$Z = R \cdot (1 + i_0 \cdot tan(\phi)); \qquad |Z| = Re\{Z\}; \tag{11}$$

$$Re\{Z\} = R \cdot 1; \qquad Im\{Z\} = R \cdot tan(\phi). \tag{12}$$

In Galilean geometry the unit circle turns into a simple vertical line. It causes the $|Z|$'s and $Re\{Z\}$'s independence from angle ϕ. Also notice that $Im\{Z\}$ can take enormously big values because of tangent function in it's expression. We used one joint normalization for quads, that represent real and imaginary parts of cells' values to show the balance between these two components of complex numbers.

On Fig. 6 you can see the modeling results for Galilean geometry case.

As you can see, in this case we have the same ring of equal high phases, but it is forming more slowly, and the values in the real parts section start to fade. When we increase $arg\{D\}$, it can be seen that while $arg\{D\} < 45^\circ$, overall imaginary component of cells is quite small with respect to the real part, but if $arg\{D\} > 45^\circ$ imaginary part starts to overbalance.

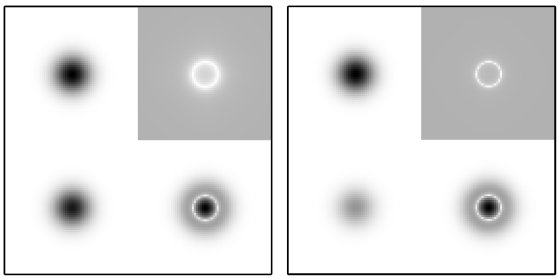

Fig. 6. 128th iteration of complex diffusion for D's phases 50° and 80° using $i^2 = 0$

4 Complex diffusion process for smoothly changing imaginary unit's square value

We can generalize our experiment by using not only imaginary units, with their squared value -1, 0 or 1. We can define new variable $i_k = i : i^2 = k$ and use some new expressions, that are right for every geometry kind:

$$Z = a + i_k \cdot b; \qquad |Z| = \sqrt{a^2 - k \cdot b^2}; \tag{13}$$

$$tan_k(\phi) = \frac{sin_k(\phi)}{cos_k(\phi)} = \frac{b}{a}, \tag{14}$$

where we define some generalized trigonometric functions:

$$Z = |Z| \cdot \left(\frac{a}{a^2 - k \cdot b^2} + i_k \cdot \frac{b}{a^2 - k \cdot b^2} \right) = |Z| \cdot (cos_k(\phi) + i_k \cdot sin_k(\phi)). \tag{15}$$

The similar approach can be seen in [9]. There are modeling results for different k values on Fig. 7. As you can see, the circle of zero phases, that we got

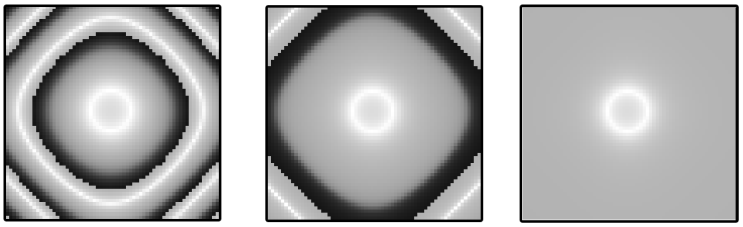

Fig. 7. Phase values of cells (i.e. only top right quad is shown) for $k = -0.25, k = -0.05$ and $k = 0$ for constant $arg\{D\} = 40.5^\circ, |D| = 0.07$ on 128th iteration

for Galilean geometry ($K = 0$), is also the first inner ring for usual Euclidean complex geometry. So Fig. 7 can bring us the conclusion: by decreasing the value of $k, i_k^2 = k$ we increase the distance between rings of zero phases for a spot that we obtain from one excited point.

5 Experiments with interference

Until that moment we were testing the behavior of a single point, that was excited in our metamedia. Now let us see what will happen if we consider the interaction of two points, that are excited at the same moment.

Fig. 8 shows the results of such experiments for the simplest case: $D \in \mathbb{R}$, $i^2 = -1$. This corresponds to diffusion equation (or the heat equation) solving, where we can see a simple spot blending without any wave processes and fluctuations.

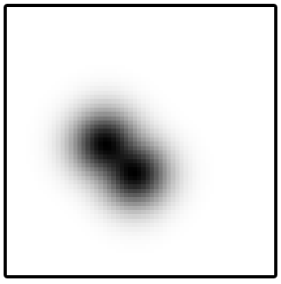

Fig. 8. Simple interference for two points in the media with $arg\{D\} = 0°$, $i^2 = -1$

More interesting results can be seen on Fig. 9, where we used a complex metamedia with $D \in \mathbb{C}$, $arg\{D\} \neq 0°$. In this case complex diffusion coefficient's phase is equal to $90° = \frac{\pi}{2}$, so the results can be considered as Schrodinger equation solution.

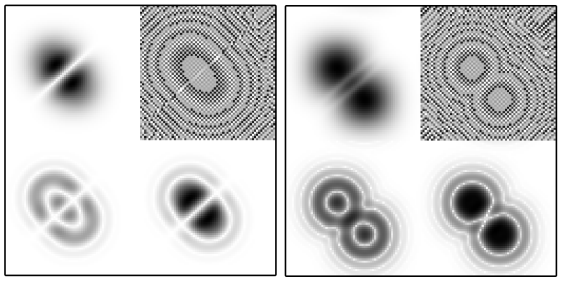

Fig. 9. Interference pictures for two points, that are located relatively close (left image) to each other and far from each other (right one). Euclidean geometry, $arg\{D\} = 90°$

It can be seen, that the output depends on the range between two points. Also a different result can be achieved if two points are excited with a relative delay (not at the same moment). It means that the phases of fluctuations inside of spots are displaced.

On Fig. 10 you can see the result of interference for metamedia with Galilean complex geometry ($i^2 = 0$). Note, that the white rings of zero phases don't intersect between each other. They have a smooth connection instead.

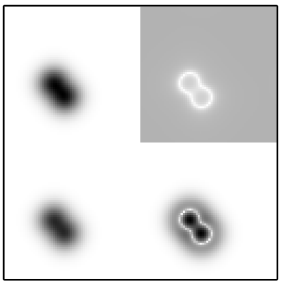

Fig. 10. Interference pictures for two points. Galilean geometry, $arg\{D\} = 60^\circ$

6 Particle movement modeling for different phases of diffusion coefficient

Very unusual and interesting results can be achieved, if we create the sequence of white points, that are lying on a circle trajectory step by step instead of using only one point at the center as an initial condition. We use well known equation for the evaluation of coordinates $(x(t), y(t))$ for next excited point's position on 2-D plane:

$$\begin{aligned} x^2(t) + y^2(t) &= R^2; \\ x(t) &= R \cdot cos(V \cdot t), \\ y(t) &= R \cdot sin(V \cdot t), \end{aligned} \tag{16}$$

where R is the radius of our circle and V is the parameter of rotation speed. This algorithm can be used for particle movement simulation within our excitable media with unusual laws.

Fig. 11 and Fig. 12 shows the algorithm functioning in action for high and low D's complex phase values. Euclidean geometry is used for this experiment, because it provides the most significant results.

The trail in phase and imaginary part quads is being formed when we increase D's phase value. Notice, that at first there are no wave interference processes in the quads, that represent real parts and absolute values of cells. When $arg\{D\}$ reaches 60° or more, we get a new process' detail. A white line, that divides a new part of a particle's trail from the older parts, comes into sight in both real and module quads.

The further increase of D's phase leads to the same interference processes between a particle's train parts, as we could see at Fig. 9. Note that the module

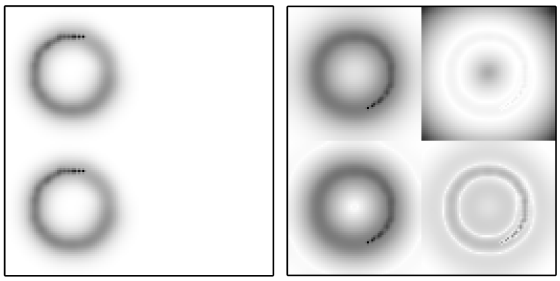

Fig. 11. Particle movement simulation on the fixed iteration for D's phases 0° (left image) and 30° (right image)

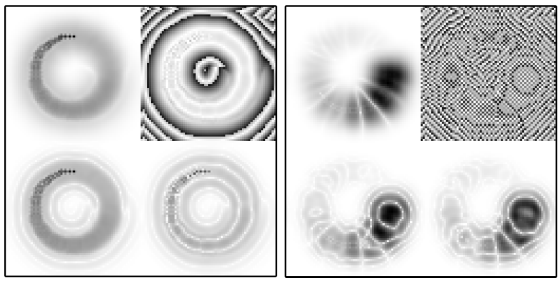

Fig. 12. Particle movement simulation taken on step 128 for D's phases 60° (left image) and 90° (right image)

values of cells, that are located close to our circle trajectory aren't constant: they are fading. It is because the fluctuations aren't in-phase. But we can suppose that it is possible to find such value of rotation speed V, that will cause mutual "maintenance" of all trail parts and will show us a steady-state.

7 Conclusion

As we can see, excitable media's reaction on the same impact is heavily dependent on complex diffuse coefficient's parameters, such as its phase. The choice of geometry type is even more important: switching its kind from one to another drastically changes the experiments' results. "Exotic" excitable medias that we have introduced in this work can provide new possibilities for quantum image processing approaches.

The future work will be related to digital image processing. Many edge detection, pattern recognition and denoising algorithms, that are implemented with Schrodinger equation for ordinary complex plane type, should be tested with Galilean and Minkowski geometry and with different D's phase values. It is possible to achieve better processing results with our new metamedia.

8 Acknowledgement

This work was supported by the Ural Federal University's Center of Excellence in "Quantum and Video Information Technologies: from Computer Vision to Video Analytics" (according to the Act 211 Government of the Russian Federation, contract 02.A03.21.0006)

References

1. *Stephen Wolfram* Cellular automata as models of complexity // Reprinted from Nature; Volume 311, No. 5985. Macmillan Journals Ltd.„ 1985. - p. 419–424.
2. *Cardenas-Barrera J., Plataniotis K.* QCA Implementation of a Multichannel Filter for Image Processing // Mathematical Problems in Engineering, 2002, Vol. 8, p. 87–99.
3. *Rosin P., Adamatzky A., Sun X.* Cellular Automata in Image Processing and Geometry — Switzerland.: Springer International Publishing, 2014. 304 p. - p. 65–80.
4. *Dmitrij Csetverikov* Basic Algorithms for Digital Image Analysis: a course. Lecture 4: Filtering II // Faculty of Informatics, Eotvos Lorand University. Budapest, Hungary.
5. *Jorg R. Welmar, John J. Tyson and Layne T. Watson* Third Generation Cellular Automaton for Modeling Excitable Media // Technical Report TR-91-11, Computer Science, Virginia Polytechnic Institute and State University, 2001.
6. *Labunets V. G.* Excitable Schrodinger metamedia // CriMiCo 2013 - 2013 23rd Internation Crimean Conference. Microwave and Telecommunication Technology, Conference proceedings. - 2013. V.I.. - p. 12.
7. *James W. Cannon* Hyperbolic Geometry // Flavors of Geometry, Volume 31. MSRI Publications, 1997. - p. 7–8.
8. *Yaglom, I. M.* Complex numbers in geometry — New York.: Academic press, 1968. 242 p. - p. 203–205
9. *Anthony A. Harkin and Joseph B. Harkin* Geometry of generalized complex numbers // Mathematics magazine, Vol. 77, No. 2. Mathematic association of America, April 2004. - p. 1–5.